Journal of Alloys and Compounds 503 (2010) 50–56

Contents lists available at ScienceDirect

Journal of Alloys and Compounds

journal homepage: www.elsevier.com/locate/jallcom

Electrochemical and surface investigation of zirconium based metallic glass $Zr_{59}Ti_3Cu_{20}Al_{10}Ni_8$ alloy in nitric acid and sodium chloride media

N. Padhy, S. Ningshen, U. Kamachi Mudali*

Corrosion Science and Technology Division, Indira Gandhi Center for Atomic Research, Kalpakkam 603102, India

ARTICLE INFO

Article history:
Received 21 March 2010
Received in revised form 27 April 2010
Accepted 2 May 2010
Available online 7 May 2010

Keywords:
Metallic glasses
Amorphisation
Corrosion
AFM

ABSTRACT

To understand the corrosion behavior of zirconium based bulk metallic glass (BMG); electrochemical, and surface investigations were carried out on $Zr_{59}Ti_3Cu_{20}Al_{10}Ni_8$ alloy in HNO_3 acid, and NaCl medium. Electrochemical studies were carried out in 1 N, 6 N and 11.5 N HNO_3 by recording open circuit potential–time, potentiodynamic polarization, and impedance characteristics. Atomic force microscope was used for *ex situ* surface morphology study of the specimens after potentiodynamic polarization in 1 N, 6 N, and 11.5 N HNO_3, and *in situ* surface morphology study by free immersion of the specimens in both 0.5 M, and 1 M NaCl solution. The results revealed attaining of steady state noble open circuit potential, wider passive region, and decrease in transpassive potential ($E_{transpass}$) with increase in HNO_3 concentration. Surface morphology in free immersion, and after polarization showed, deep pit propagation in both 0.5 M, and 1 M NaCl solution, and aggressive surface dissolution in HNO_3 medium.

1. Introduction

Developed in the early 90s, zirconium based, multi component bulk metallic glasses (BMGs) are finding increasing applications due to their high glass forming ability, high thermal stability and improved mechanical properties [1–4]. Corrosion resistance, chemical stability and oxidation behavior are the properties to be assessed for its many fold application as structural engineering components in aggressive corrosive media. Major concerns for these materials are high pitting susceptibility in chloride containing environment, viability of good mechanical properties, and prolonged service in the presence of corrosive environment [5–7]. To date significant efforts have been made to evaluate the corrosion resistance of zirconium based bulk metallic glass. Gebert et al. [8] have predicted pronounced selective dissolution of glassy phase matrix, and poor repassivation ability in chloride containing environment. Kamachi Mudali et al. proposed a mechanism by which localized corrosion attack can take place for Zr-based BMGs in chloride medium [5,9,10]. Morrosion et al. [11] have found significant susceptibility of $Zr_{41.2}Ti_{13.8}Ni_{10}Cu_{12.5}Be_{22.5}$ alloy to pitting in 0.6 M NaCl medium. Zander and Köster [12] have compared the corrosion behavior of nano-crystaline zirconium glassy alloys with crystalline counter parts. Schroeder et al. [13] have reported marginal improvement in pitting corrosion resistance for Zr-based metallic glass than its crystallized counterparts in 0.5 M NaCl, and *in situ* element specific and time resolved corrosion investigation by Homazava et al. [14] have predicted high corrosion resistance for $Zr_{58.5}Cu_{15.6}Ni_{12.8}Al_{10.3}Nb_{2.8}$ in 1 M HCl, and 1 M HNO_3 acidic media due to change in elemental composition in oxide film. However, many details are still not available regarding viability of these structural amorphous materials in aggressive environment, for application in nuclear industry.

Nuclear fuel reprocessing demands materials that should possess high corrosion resistance, good mechanical properties, and long service life for economical extraction of useful radionuclide from spent nuclear fuel. Nitric acid is used from dilute to concentrated, and from room temperature to boiling condition as the process medium for fuel reprocessing purpose [15]. Besides this, as most reprocessing plants are located near saline atmosphere, chloride content in the surrounding environment acts as a life-limiting factor for many of the structural components. Present generation of reprocessing plants uses AISI type 304L SS, and its upgraded varieties, titanium and its alloys, and zirconium as structural materials for nitric acid services. However, problems associated with such type of materials are many such as, sensitization related corrosion problems in welds of dissimilar metals, grain boundary dissolution as well as intergranular corrosion in stainless steel components, vapor phase corrosion of titanium, and stress corrosion cracking of zirconium in hot nitric acid [15–19]. All these corrosion related problems limit the life span of structural materials, and hence has direct impact on plant production. Thus, the material selection for fuel reprocessing plant is a tedious on-going process in the hunt for better materials that can provide longer life to the plant [15].

* Corresponding author. Tel.: +91 44 27480121; fax: +91 44 27480301.
E-mail address: kamachi@igcar.gov.in (U. Kamachi Mudali).

0925-8388/$ – see front matter © 2010 Elsevier B.V. All rights reserved.
doi:10.1016/j.jallcom.2010.05.002

BMGs being amorphous in nature do not possess grain boundaries, and second phase precipitate. Mechanical properties such as ductility, plasticity and fatigue behavior are comparable to that of high strength crystalline alloys which are adequate to meet the stringent manufacturing requirements for various components in reprocessing plant [20–22]. Main advantage with such type of material lies in that, they can be cast into different shapes and dimensions for critical applications demanding superior corrosion resistance, better resistance to cavitation corrosion, erosion and wear characteristics [23–25]. Nevertheless, concerns too exist regarding their thickness for large-scale industrial application. However, these materials can find application in combination with traditional alloys, and work is on progress in this direction for evaluating their corrosion resistance, and workability in nuclear fuel reprocessing environment [26,27].

In the present work an attempt has been made to investigate the electrochemical properties of zirconium based BMGs of type Zr–Cu–Al–Ni–X alloys. Selection of such type of material for nitric acid applications is due to better passivation property of zirconium and aluminum, improved strength due to presence of nickel, and high glass forming ability of copper. The addition of X (Ti, Nb) up to 5 at.% results in significant improvement in corrosion resistance, however with increasing addition of Ti and Nb significant reduction in glass forming ability is also observed [28,29]. Hence, this class of material can be ideal candidate material for possible potential future application in nuclear fuel reprocessing plants. The aim of present work is to evaluate the corrosion behavior and passivating nature of $Zr_{59}Ti_3Cu_{20}Al_{10}Ni_8$ alloy in 1 N, 6 N, and 11.5 N nitric acid, and the pitting susceptibility in 0.5 M, and 1 M NaCl solution by electrochemical investigations, and surface morphological studies.

2. Experimental

2.1. Specimen preparation

Material chosen for the present study was zirconium based metallic glass alloy of the composition $Zr_{59}Ti_3Cu_{20}Al_{10}Ni_8$ (wt%). Amorphous alloy of the aforementioned nominal composition was prepared by melting pure elements of purity 99.99% in arc melting furnace on a water-cooled copper mould in a highly purified argon-gettered atmosphere. The ingots obtained were subsequently remelted several times to obtain compositional homogeneity, and to control the impurities especially oxygen. Glassy ribbons of thickness 40 μm, and 5 mm width were prepared from the arc-melted pre alloy using single roller melt spinning under argon atmosphere. The details of the equipments involved, and preparation conditions of the alloy can be found elsewhere in Ref. [30].

2.2. Thermal and microstructural analysis

The thermal behavior, and microstructural analysis of glassy ribbons prepared were characterized using differential scanning calorimetry (DSC), and X-ray diffraction (XRD). The thermochemical parameters such as glass transition temperature (T_g), under-cooled region (ΔT) were examined using a PerkinElmer DSC7 differential scanning calorimetry at a heating rate of 40 K/min in purified argon flow. Separate DSC scan was carried out for three different samples weighing about 5 mg by cutting from glassy ribbon. The amorphous nature of the prepared samples was examined using a Philips PW 1050 X-ray diffractometer with CuKα radiation ($\lambda = 1.5418$ Å) with scattering angle (2θ) between 25° and 65°.

2.3. Electrochemical investigations for corrosion study

The specimens for electrochemical studies were prepared by polishing 5 mm × 5 mm glassy ribbon samples mechanically with 1200 grade emery paper (SiC), and then polished in 1 μm alumina paste. All the specimens after polishing were ultrasonically cleaned in acetone, and then with double distilled water.

Electrochemical investigations were carried out in 1 N, 6 N, and 11.5 N HNO_3 using three-electrode electrochemical cell consisting of Pt counter electrode, Ag/AgCl reference electrode, and sample as working electrode for studying open circuit potential (OCP) versus time, electrochemical impedance, and potentiodynamic polarization behavior. The samples were mounted in a probe holder with adhesive, exposing the top surface inside the test solution. Special care was taken to prevent seeping of electrolyte to the interface of sample, and probe holder by filling the gap with an organic resin, and tightly covering with Teflon tape. The electrochemical test solution was prepared form analytical grade chemical reagent with double distilled water. All the electrochemical potential mentioned here are with respect to standard Ag/AgCl reference electrode.

OCP-time measurement provides insight into the instantaneous electrochemical process occurring in the alloy surface without any external disruption, and is important for determining tendency of materials to free corrosion. For the present study, free corrosion potential was obtained by immersing the samples for 1 h without any electrochemical control. Five set of experiments were carried out in each of the above mentioned test solutions to check the reproducibility. Electrochemical impedance analysis was carried out using Solartron 1255 Frequency Response Analyzer (FRA) combined with Solartron 1287 electrochemical interface after steady open circuit potential condition was attained. EIS measurement was carried out in the frequency range of 0.1 Hz to 10^5 Hz with 10 points per decade by applying oscillating potential having 5 mV amplitude. The impedance responses obtained over the applied frequency range were analyzed by Nyquist plot. The EIS results were interpreted by using two different equivalent circuit models of $[R_s\ (C_{dl}||R_P)]$ and $[R_s\ (C_1||R_1)\ (C_2||R_2)]$ for fitting and analyzing the impedance spectra. Where R_s is the solution resistance, C_{dl} is the double layer capacitance, C_1 and R_1 are the film capacitance and film resistance, and C_2 and R_2 is the interfacial process of double layer capacitance and charge transfer resistance, respectively. In 1 N and 6 N nitric acid only one time constant was observed hence the equivalent circuit arrangements $[R_s\ (C_{dl}||R_P)]$ was used. However, in 11.5 N nitric acid since two time constant was observed, the equivalent circuit model of $[R_s\ (C_1||R_1)\ (C_2||R_2)]$ was used for fitting impedance data. The selection of these circuit elements was a compromise between a reasonable fitting of the experimental value and minimum components involved in the equivalent circuit.

After analyzing open circuit potential, and electrochemical impedance, potentiodynamic polarization test was carried out in aforementioned nitric acid solutions at room temperature using Solartron 1287 electrochemical interface associated with standard three-electrode cell. The electrode potential was ramped at a rate of 0.1667 mV/s from 0.4 V up to 1.6 V. Five sets of experiments were conducted in each solution, and all the polarization plots were almost reproducible. The electrochemical solution used for the tests was not de-aerated as the experiments were carried out in simulated plant condition. From the polarization study quantitative values of corrosion related parameters such as corrosion potential (E_{corr}), corrosion current density (I_{corr}), passive current density (I_{pass}), and transpassive potential ($E_{transpass}$) were obtained to understand the propensity of glassy amorphous material to passivation, and corrosion susceptibility. Tafel like regions cannot be seen clearly in the present polarization plots. The quantitative values of corrosion related parameters were obtained by fitting Tafel lines in linear segments of current–voltage curve within 100 mV of corrosion potential. During potentiodynamic polarization, the potential at which there was a monotonic increase in the anodic current exceeding 25–100 μA in aforementioned nitric acid solution was termed as the transpassive potential ($E_{transpass}$). The values given for the above corrosion related parameters are the mean value of all the experiments conducted in a particular solution with mentioned standard deviation.

2.4. Surface morphology study by AFM

Surface morphology investigations of the as polished sample, *in situ* study by free immersion in 0.5 M, and 1 M NaCl solutions, and *ex situ* study after anodic polarization tests were carried out using NT-MDT (Molecular Devices and Tools for Nano Technology) make atomic force microscope (Solver ProEC). Prior to surface morphological measurements, the scanner was calibrated by standard grating, and reference images of the sample were taken at different locations of the sample to ensure the surface homogeneity. The *in situ* morphology study in sodium chloride solution without any electrochemical control was carried out by using a special cell made up of titanium having volume capacity of 2 ml. Samples having size 5 mm × 5 mm were kept fixed by pressing two clips made up of platinum inside the solution, and the topography was continuously monitored at an interval of 30 min to detect morphological changes occurring on the surface over time. The experiment was repeated three times in both the concentrations of the sodium chloride solution to average out the surface morphology. For *ex situ* morphological study after potentiodynamic polarization in nitric acid, the samples were immediately removed from holder once the experiment was over, ultrasonically cleaned with double distilled water, dried and examined. Several topographic images were collected for each of the polarized samples at different locations to examine the surface uniformity. All the measurements were carried out in semi-contact mode using standard conical silicon tip attached to cantilever having force constant 5 nN/m with frequency range from 50 Hz to 150 Hz in ambient condition. The typical curvature of radius of tip is 10 nm, and the cone angle is less than 22°.

3. Results and discussion

3.1. Physical characterization

The results obtained for physical characterization of $Zr_{59}Ti_3Cu_{20}Al_{10}Ni_8$ alloy using DSC are shown in Fig. 1. DSC

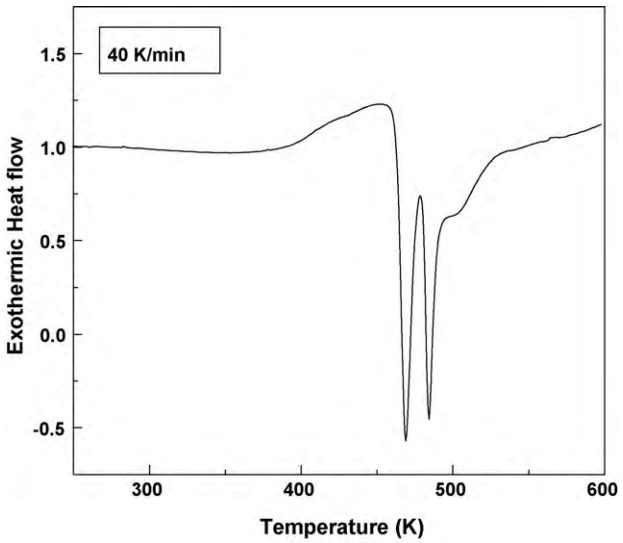

Fig. 1. DSC scan for a melt-spun amorphous $Zr_{59}Ti_3Cu_{20}Al_{10}Ni_8$ alloy sample recorded at a heating rate of 40 K/min.

profile marked the presence of glass transition (T_g) followed by two crystallization peaks T_{x1}(onset) and T_{x2} (onset) during heating at 40 K/min. The glass transition, and two crystallization peak temperatures were found to be occurring around 416 K, 468 K and 485 K, respectively. The super-cooled region ($\Delta T = T_{x1} - T_g$) value was found to be 52 K indicating stability of glass transition regime. The variation in the transformation temperatures for glass transition, and crystallization peak temperature was found to be within the range of ±4 K at a constant heating rate of 40 K/min for three different samples. The occurrence of two crystallization peaks is an indicative of successive formation of different phases. The XRD pattern of $Zr_{59}Ti_3Cu_{20}Al_{10}Ni_8$ alloy showed only broad spectrum indicating amorphous nature (Fig. 2).

3.2. Open circuit potential–time measurement

The open circuit potential (OCP) versus time plots during the immersion for 1 h in 1 N, 6 N, and 11.5 N nitric acid medium are shown in Fig. 3. The OCP attained noble and steady state in all concentration of nitric acid just after immersion indicating stable, and rapidly forming passive film. Noble OCP value in all concentrations

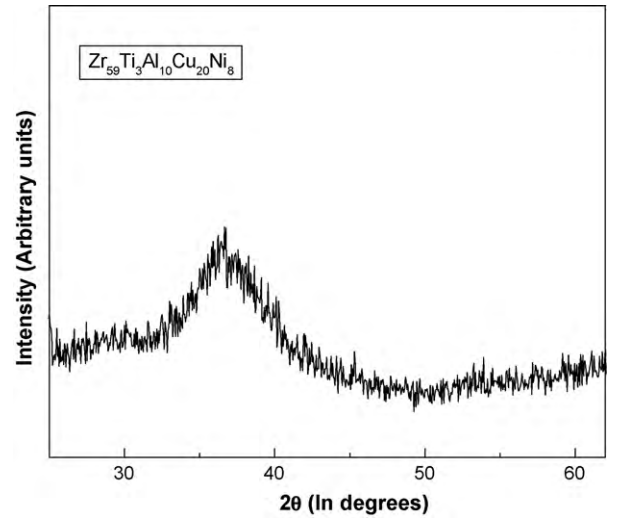

Fig. 2. XRD profile of $Zr_{59}Ti_3Cu_{20}Al_{10}Ni_8$.

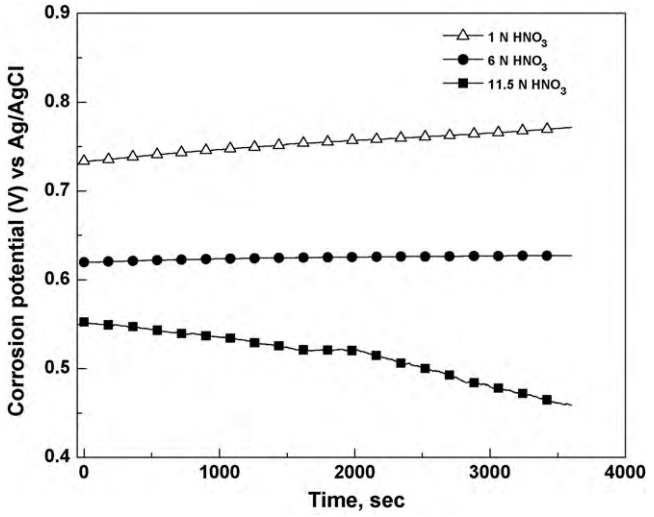

Fig. 3. Open circuit potential of $Zr_{59}Ti_3Cu_{20}Al_{10}Ni_8$ alloy in 1 N, 6 N, and 11.5 N HNO_3.

of nitric acid is ascribed to thick natural oxide layer of zirconium and aluminum (ZrO_2, Al_2O_3) forming barrier type passive film [8]. The OCP value shifted towards less noble value with increase in nitric acid concentration. The lower OCP value observed at higher concentrations is attributed to the higher oxidizing power of nitric acid leading to less stable passive film on the surface. Structural heterogeneities such as micro-pores, and nano-voids do exist in amorphous glassy materials, where passive film is largely non-homogenous. These regions are of high energy, and are the weaker regions providing assessable sites for the initiation of passive film dissolution. As a result, not only the passive film is unstable in these regions, but also susceptible to rupture leading to its breakdown. Cumulative effect of the above processes can lead to an unstable passive film, and hence the observed trend in shift of open circuit potential value in different concentrations of nitric acid.

3.3. Potentiodynamic polarization results

The results for potentiodynamic anodic polarization study in 1 N, 6 N, and 11.5 N nitric acid are as shown in Fig. 4. The polarization plots did not revealed any active-passive transition behavior as without showing any active peak it translated into passive

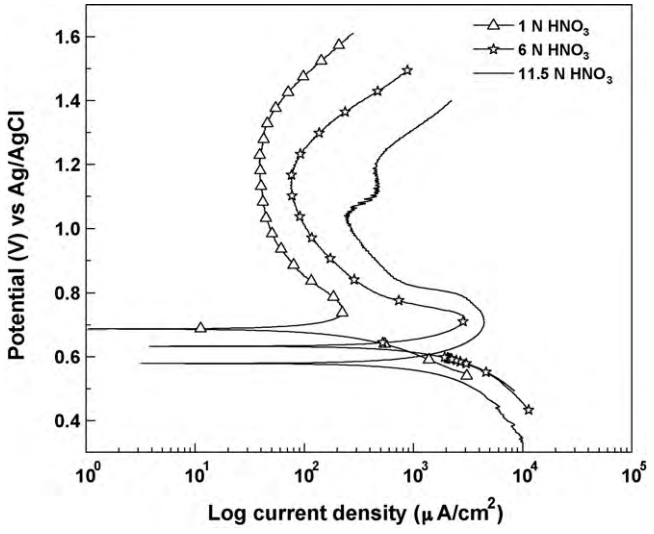

Fig. 4. Potentiodynamic polarization plots for $Zr_{59}Ti_3Cu_{20}Al_{10}Ni_8$ alloy in 1 N, 6 N, and 11.5 N HNO_3.

Table 1
Polarization parameters of $Zr_{59}Ti_3Cu_{20}Al_{10}Ni_8$ alloy in 1 N, 6 N and 11.5 N HNO_3.

Nitric acid concentration	E_{Corr} V vs Ag/AgCl	I_{Corr} ($\mu A/cm^2$)	I_{Pass} ($\mu A/cm^2$)	$E_{tranpass}$ V vs Ag/AgCl
1 N HNO_3	0.68	5.5×10^1	1×10^2	1.4
6 N HNO_3	0.63	1.4×10^2	2.5×10^2	1.3
11.5 N HNO_3	0.57	3×10^2	4×10^2	1.1

region followed by transpassive regime in all the concentration of test solution. All the corrosion related parameters obtained from the polarization plots (E_{corr}, I_{corr}, I_{pass} and $E_{transpass}$) are shown in the Table 1. As mentioned earlier the values are mean of all the experiments conducted in a particular solution, and the standard deviation for the E_{corr}, I_{corr}, I_{pass} and $E_{transpass}$ in all the concentrations are within ±15 mV, ±10 $\mu A/cm^2$, ±20 $\mu A/cm^2$ and ±25 mV, respectively. In 1 N nitric acid the polarization curve exhibited wider passive range with low passive current density, and higher transpassive potential. At higher concentrations of nitric acid (6 N, 11.5 N) the passive range narrowed down with decrease in transpassive potential, and increase in passive current density. In 11.5 N nitric acid concentration the polarization curve revealed a second passive region which is an indicative of change in passive film property due to auto-catalytic reduction of nitric acid at higher concentration [15,17].

Surface analysis by Gebert et al. [8,31] using auger electron spectroscopy (AES) for similar BMG alloy has shown the existence of natural oxide layer mainly consisting of ZrO_2 and small quantity of Al_2O_3 having thickness of 8–10 nm. The decrease in passive current density as well as transpassive potential depends upon the homogeneity of passive film which in turn depends upon the electrochemical environment. As the concentration of nitric acid increase, the oxidizing nature of the electrochemical test solution also increases leading to dissolution of passive film as well as change in the chemical state of the alloying elements which in turn alters the nature of passive film. At higher concentrations of nitric acid (11.5 N) appearance of second passive region indicates conversion of metastable passive film to a less protective film. Polarization study carried out by Kamachi Mudali et al. [9] in acidic media has also revealed the existence of second passive region suggesting alteration in chemical composition of oxide layer within the passive film. The change over of passive film property is due to selective oxidation of its alloying element in acidic environment leading to formation of corrosive products on the surface. Nevertheless, structural heterogeneities such as nano-size crystallites, nano-phase precipitates and various types of multiphase particles engrafted in amorphous material makes the passive film weaker by reducing metal–oxide bonding capability. Comparative study made by Chieha et al. [32] on corrosion resistance of $Zr_{52.5}Cu_{17.9}Ni_{14.6}Al_{10}Ti_5$, and 304L stainless steel in different acidic media revealed the better corrosion resistance for zirconium based BMGs as compared to 304L stainless steel. In 1 N HNO_3, and 1 N H_2SO_4 these alloys exhibited wider passive region, and lower passive current densities confirming the easily attained passive nature.

3.4. Electrochemical impedance analysis

The Nyquist plots during electrochemical impedance analysis under open circuit potential condition in 1 N, 6 N, and 11.5 N HNO_3 are shown in Fig. 5. As can be seen from the plots, distinct difference was observed depending upon the nitric acid concentrations indicating differences in the stability of passive film. All the Nyquist plots showed unfinished semi-circular arc, and the polarization resistance and double layer capacitance obtained by fitting in individual concentration are shown in Table 2. In 1 N HNO_3 higher polarization resistance, and lower double layer capacitance were observed as compared to 6 N, and 11.5 N HNO_3. The higher polarization resistance in impedance spectra is consistent with polarization behavior of low passive current density, and higher transpassive potential in 1 N HNO_3. High value of R_P in lower concentration of nitric acid is an indication of good passive film stability, and is due to less diffusion of ionic species or less charge transfer, and their accumulation across the film–solution interface. However, in 11.5 N HNO_3 two time constant capacitive loops were observed in consistent with two passive region in polarization curve, both are at low frequencies and the value of polarization resistance was much lower as compared to 1 N and 6 N HNO_3. The lower value of polarization resistance, and occurrence of two time constants in 11.5 N HNO_3 are attributed to higher charge transfer across the film–solution interface due to catalytic oxidation of alloying elements in the passive film. Oxidation of alloying elements such as Zr(II), and Al(III) due to catalytic reduction of nitric acid can change the passive film character leading to less stable passive film at higher concentration of nitric acid. The occurrence of two time constants is unique feature of change in passive film property.

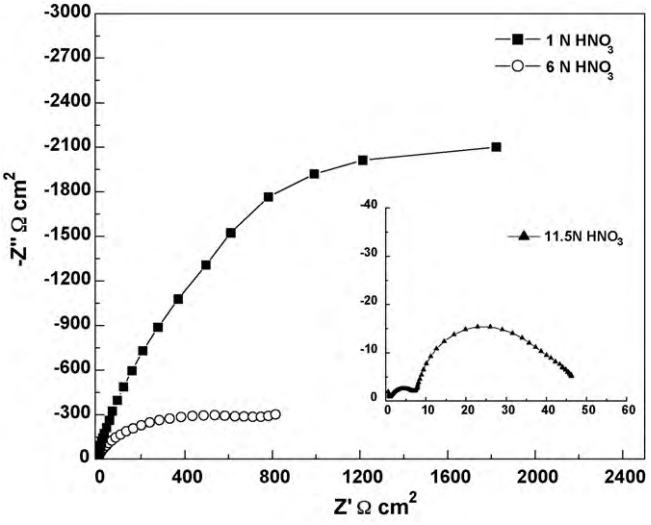

Fig. 5. Nyquist plot for $Zr_{59}Ti_3Cu_{20}Al_{10}Ni_8$ alloy in 1 N, 6 N, and 11.5 N HNO_3.

Table 2
EIS fitted value of $Zr_{59}Ti_3Cu_{20}Al_{10}Ni_8$ alloy in 1 N, 6 N and 11.5 N HNO_3 measured at OCP condition.

Nitric acid concentration	R_S ($\Omega\,cm^2$)	R_p ($\Omega\,cm^2$)		C_{dl} (F/cm^2)	
1 N HNO_3	0.22	2162		9.82×10^{-5}	
6 N HNO_3	0.58	892		8.32×10^{-4}	
11.5 N HNO_3	1.17	10.1(R_1)	45(R_2)	1.6×10^{-6}(C_1)	3.10×10^{-4}(C_2)

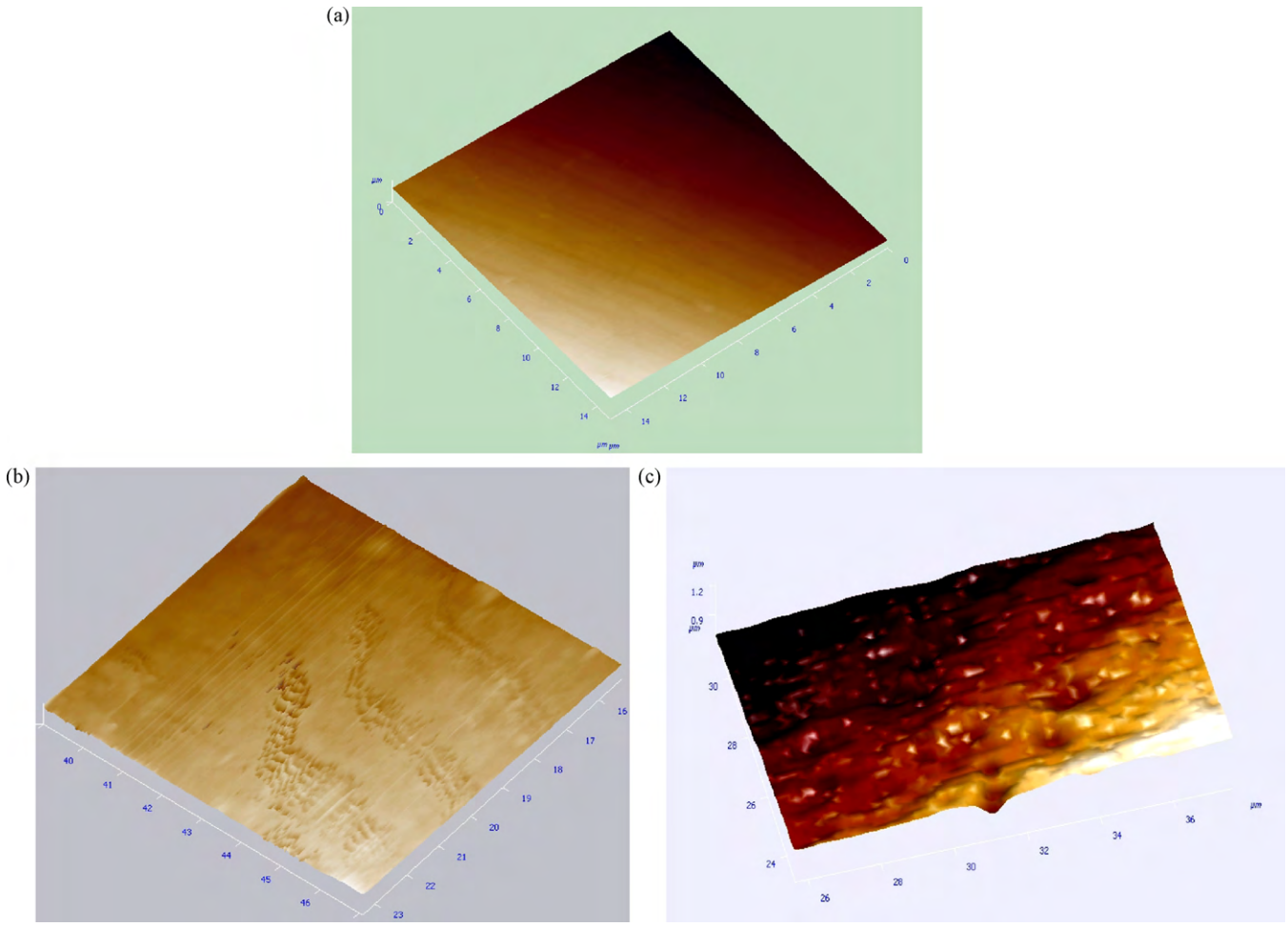

Fig. 6. Surface morphology of $Zr_{59}Ti_3Cu_{20}Al_{10}Ni_8$ (a) as polished, (b) 10 h of immersion in 0.5 M NaCl, and (c) 7 h of immersion in 1 M NaCl.

3.5. *Ex situ and in situ study of surface morphology by AFM*

The surface morphology study for pitting corrosion in 0.5 M, and 1 M NaCl in free immersion conditions, and morphological examination after anodic polarization in 1 N, 6 N, and 11.5 N HNO_3 were carried out using atomic force microscope. Fig. 6 shows the surface morphology of (a) as polished alloy surface, (b) surface topography in 0.5 M NaCl after 10 h of immersion, and (c) after 7 h of immersion in 1 M NaCl, respectively. The surface morphology studies revealed the process of pit initiation, their growth, and propagation over the alloy surface. The pit morphology altered with time starting from pit nuclei initiation, and channel like propagation in a river flow manner in the same direction (Fig. 6(b)) to the homogenous growth in pit morphology (Fig. 6(c)) at higher concentration of sodium chloride solution (1 M NaCl). In Zr-based amorphous BMGs, propensity to pitting is a localized phenomenon mainly due to chloride ion, and mostly occurring at the surface defects such as inhomogenities formed during casting process, bimetallic phases, and defects generated during mechanical sample preparation. Once pitting initiated, it propagates by selective dissolution of less noble metals (Zr, Al) due to auto-catalytic reaction with chloride ions giving the appearance of dip channel like pit as observed in Fig. 6(b) [5,10]. Surface investigation using AES regarding the elemental analysis of passivated, and corroded regions has revealed the enrichment of Cu beneath the passive layer. Moreover, compounds of Cu and Cl have been detected in pit bottom which makes the passive film weaker, giving preferential bias to aggressive ions [33]. As compared to 0.5 M NaCl, in 1 M NaCl the observed pit propagation is well ordered, and in similar nature with each pit growing from the next leaving a microspace in between. The homogenous nature of growth is an indication of dependence of pit growth with time of immersion as well as concentration of sodium chloride solution.

The surface morphology of $Zr_{59}Ti_3Cu_{20}Al_{10}Ni_8$ alloy after anodic polarization in 1 N, 6 N, and 11.5 N HNO_3 are as shown in Fig. 7(a)–(c). The morphological features after polarization in different nitric acid media revealed roughening of surface in 1 N HNO_3 (Fig. 7(a)), to uniform surface dissolution in 6 N HNO_3 (Fig. 7(b)), to aggressive surface dissolution giving the appearance of trench like structure in 11.5 N HNO_3 (Fig. 7(c)). The extent of surface dissolution depends on the protecting power of the oxide film as well as the concentration of nitric acid medium. In 1 N HNO_3 the observed surface roughening, and lack of surface dissolution process indicates greater passive film stability over a wide potential region at lower concentration. The minor surface roughening observed can be due to inhomogenities present on the surface. In 6 N HNO_3 the morphology became more irregular with prominent dissolution and formation of mound like surface due to lower transpassive potential, and higher anodic process catalyzed by nitric acid [34]. The surface topography of the alloy after anodic polarization in 11.5 N HNO_3 showed strong selective dissolution with the formation of trench like surface morphology.

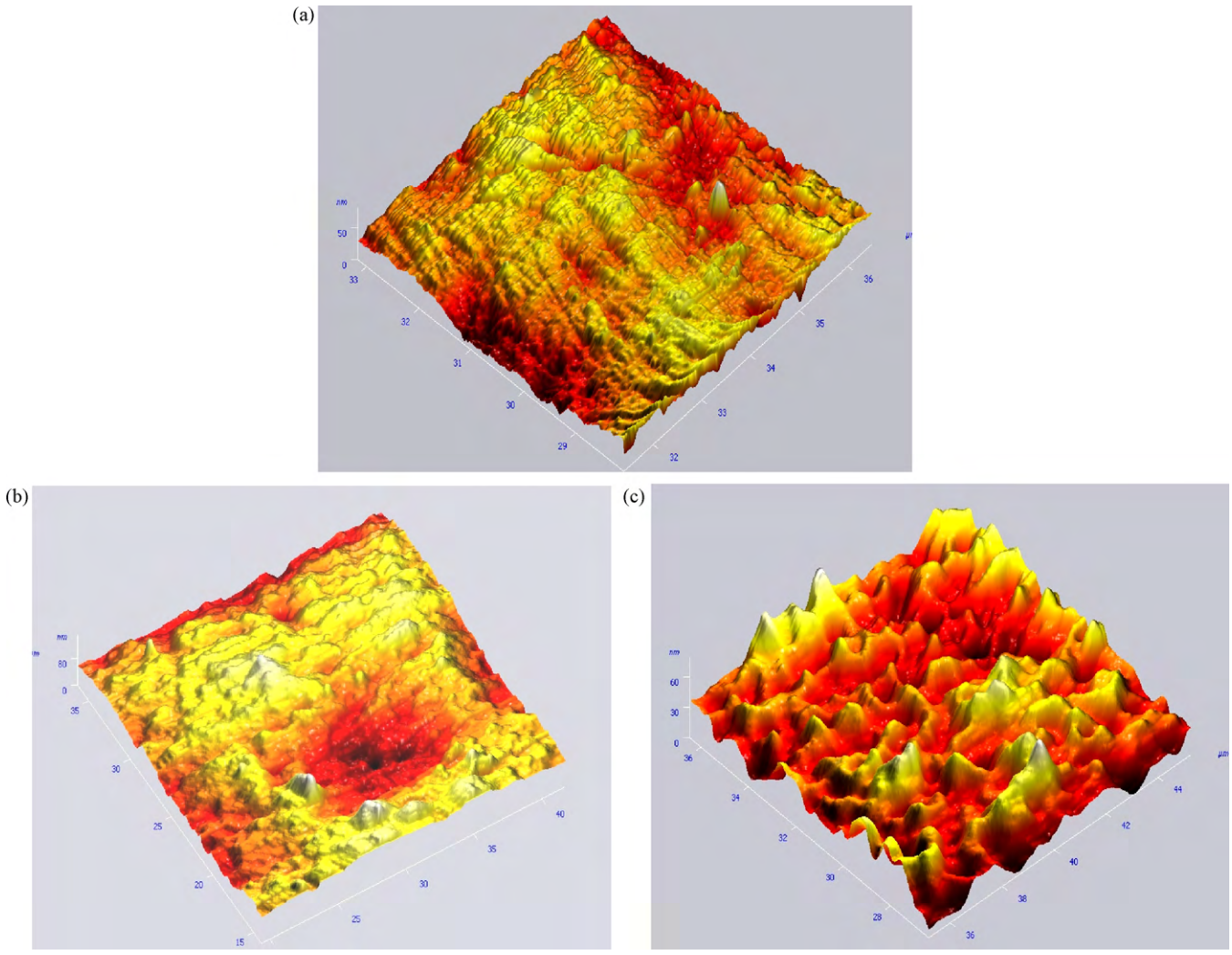

Fig. 7. Surface morphology of $Zr_{59}Ti_3Cu_{20}Al_{10}Ni_8$ after potentiodynamic polarization in (a) 1 N HNO_3, (b) 6 N HNO_3, and (c) 11.5 N HNO_3.

4. Conclusions

The following are the major conclusions from the present study on "Electrochemical and surface investigation of zirconium based metallic glass $Zr_{59}Ti_3Cu_{20}Al_{10}Ni_8$ alloy in nitric acid and sodium chloride media".

1. The open circuit potential–time measurements in 1 N, 6 N, and 11.5 N HNO_3 showed stable passive film formation. The decrease in OCP value with increase in nitric acid indicates dependence of film stability upon nitric acid concentrations.
2. The potentiodynamic polarization results showed decrease in transpassive potential with increase in nitric acid concentration indicating lower corrosion resistance at higher concentration of nitric acid.
3. Electrochemical impedance analysis showed good passive film stability in 1 N, and 6 N nitric acid, however in 11.5 N nitric acid; Nyquist plot showed two time constants which is distinct feature of change in passive film property in oxidizing environment of nitric acid.
4. *In situ* surface morphology study by AFM in 0.5 M NaCl, and 1 M NaCl showed pit nuclei initiation, and their growth indicating susceptibility of $Zr_{59}Ti_3Cu_{20}Al_{10}Ni_8$ to pitting in chloride containing environment.
5. Surface morphology after potentiodynamic polarization showed surface roughening, corrugated surface morphology, and uniform surface dissolution of the alloy depending upon nitric acid concentration.

Acknowledgement

Thanks are due to Dr. A. Gebert, IFW, Dresden for providing the BMG amorphous alloy for the investigation.

References

[1] A. Inoue, Mater. Sci. Eng. A 16 (2004) 375–377.
[2] J.R. Scully, A. Gebert, J.H. Payer, J. Mater. Res. 22 (2007) 302–313.
[3] D. Fátay, J. Gubicza, P. Szommer, J. Lendvai, M. Blétry, P. Guyot, Mater. Sci. Eng. A 1001 (2004) 387–389.
[4] N. Eliaz, D. Eliezer, E. Abramov, D. Zander, U. Köster, J. Alloys Compd. 305 (2000) 272–281.
[5] U. Kamachi Mudali, S. Baunack, J. Eckert, L. Schultz, A. Gebert, J. Alloys Compd. 377 (2004) 290–297.
[6] V. Schroeder, R.O. Ritchie, Acta Mater. 54 (2006) 1785–1794.
[7] S. Buzzi, K. Jin, Peter J. Uggowitzer, S. Tosatti, I. Gerber, J.F. Loffler, Intermet 14 (2006) 729–734.
[8] A. Gebert, U. Kuehn, S. Baunack, N. Mattern, L. Schultz, Mater. Sci. Eng. A 415 (2006) 242–249.
[9] U. Kamachi Mudali, S. Scudino, U. K€uhn, J. Eckert, A. Gebert, Scripta Mater. 50 (2004) 1379–1384.
[10] U. Kamachi Mudali, S. Scudino, U. Kuhn, J. Eckert, L. Schultz, A. Gebert, Trans. IIM 59 (2006) 123–138.

[11] M.L. Morrisona, R.A. Buchanan, A. Peker, W.H. Peter, J.A. Horton, P.K. Liaw, Intermet 12 (2004) 1177–1181.
[12] Daniela Zander, Uwe Köster, Mater. Sci. Eng. A 53 (2004) 375–377.
[13] V. Schroeder, C.J. Gilbert, R.O. Ritchie, Scripta Mater. 38 (1998) 1481–1485.
[14] N. Homazava, A. Shkabko, D. Logvinovich, U. Krahenbuhl, A. Ulrich, Intermet 16 (2008) 1066–1072.
[15] Baldev Raj, U. Kamachi Mudali, Prog. Nucl. Energy 48 (2006) 283–313.
[16] U. Kamachi Mudali, B.M. Anand Rao, K. Shanmugam, R. Natrajan, Baldev Raj, J. Nucl. Mater. 321 (2003) 40–48.
[17] P. Fauvet, F. Balbaud, R. Robin, Q.-T. Tran, A. Mugnier, D. Espinoux, J. Nucl. Mater. 375 (2008) 52–64.
[18] U. Kamachi Mudali, R.K. Dayal, J.B. Gnanamoorthy, J. Nucl. Mater. 203 (1993) 73–82.
[19] Hiroo Nagano, Haruhiko Kajimura, Kazuo Yamanaka, Mater. Sci. Eng. A 98 (1995) 127–134.
[20] W.H. Jiang, G.J. Fan, H. Choo, P.K. Liaw, Mater. Lett. 60 (2006) 3537–3540.
[21] Wenbo Dong, Haifeng Zhang, Jing Cai, Wensheng Sun, Aimin Wang, Hong Li, Zhuangqi Hu, J. Alloys Compd. 425 (2006) L1–L4.
[22] G.Y. Wang, P.K. Liaw, Y. Yokoyama, A. Inoue, C.T. Liu, Mater. Sci. Eng. A 494 (2008) 314–323.
[23] Cang Fan, Laszlo J. Kecskes, Dong-Chun Qiao, Hahn Choo, Peter K. Liaw, J. Non-Cryst. Solids 352 (2006) 174–179.
[24] G.Q. Zhang, X.J. Li, M. Shao, L.N. Wang, J.L. Yang, L.P. Gao, L.Y. Chen, C.X. Liu, Mater. Sci. Eng. A 475 (2008) 124–127.
[25] D. Drozdz, R.K. Wunderlich, H.-J. Fecht, Wear 262 (2007) 176–183.
[26] C. Qin, K. Asami, H. Kimura, W. Zhang, A. Inoue, Electrochem. Commun. 10 (2008) 1408–1410.
[27] C. Qin, K. Asami, H. Kimura, W. Zhang, A. Inoue, Electrochim. Acta 10 (2008) 1408–1410.
[28] M.K. Tam, S.J. Pang, C.H. Shek, J. Phys. Chem. Solids 67 (2006) 762–766.
[29] H. Men, S.J. Pang, T. Zhang, Mater. Sci. Eng. A 408 (2005) 326–329.
[30] A. Gebert, K. Buchholz, A. Leonhard, K. Mummert, J. Eckert, L. Schultz, Mater. Sci. Eng. A 267 (1999) 294–300.
[31] S. Baunack, U. Kamachi Mudali, A. Gebert, Appl. Surf. Sci. 252 (2005) 162–166.
[32] T.C. Chieha, J. Chua, C.T. Liub, J.K. Wua, Mater. Lett. 57 (2003) 3022–3025.
[33] B.A. Green, H.M. Meyer, R.S. Benson, Y. Yokoyama, P.K. Liaw, C.T. Liu, Corros. Sci. 50 (2008) 1825–1832.
[34] S. Ningshen, U. Kamachi Mudali, G. Amerendra, Baldev Raj, Corros. Sci. 51 (2009) 322–329.